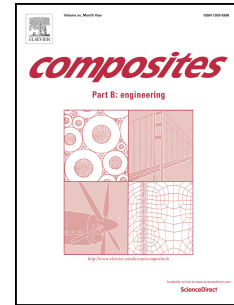


# Accepted Manuscript

Snap-through behaviour of a bistable structure based on viscoelastically generated prestress

Bing Wang, Chao Ge, Kevin S. Fancey



PII: S1359-8368(16)31730-9

DOI: [10.1016/j.compositesb.2017.01.069](https://doi.org/10.1016/j.compositesb.2017.01.069)

Reference: JCOMB 4880

To appear in: *Composites Part B*

Received Date: 8 September 2016

Revised Date: 7 December 2016

Accepted Date: 8 January 2017

Please cite this article as: Wang B, Ge C, Fancey KS, Snap-through behaviour of a bistable structure based on viscoelastically generated prestress, *Composites Part B* (2017), doi: 10.1016/j.compositesb.2017.01.069.

This is a PDF file of an unedited manuscript that has been accepted for publication. As a service to our customers we are providing this early version of the manuscript. The manuscript will undergo copyediting, typesetting, and review of the resulting proof before it is published in its final form. Please note that during the production process errors may be discovered which could affect the content, and all legal disclaimers that apply to the journal pertain.

**Snap-through behaviour of a bistable structure based on viscoelastically generated prestress**Bing Wang<sup>1</sup>, Chao Ge<sup>1,2</sup>, Kevin S. Fancey<sup>1\*</sup><sup>1</sup>School of Engineering, University of Hull, HU6 7RX, UK<sup>2</sup>School of Mechatronics Engineering, Beijing Institute of Technology, Beijing, 100081, China**Abstract**

A novel form of shape-changing bistable structure has been successfully developed through the use of viscoelastically generated prestress. Bistability is achieved through pairs of deflecting viscoelastically prestressed polymeric matrix composite (VPPMC) strips, which are orientated to give opposing cylindrical configurations within a thin, flexible resin-impregnated fibreglass sheet. This arrangement enables the structure to ‘snap through’ between one of two states by external stimulation. Deflection from the VPPMC strips occurs through compressive stresses generated from the non-uniform spatial distribution of nylon 6,6 fibres undergoing viscoelastic recovery. In this study, snap-through behaviour of the bistable structure is investigated both experimentally and through finite element (FE) analysis. By using experimental results to calibrate FE parameter values, the modelling has facilitated investigation into the development of bistability and the influence of modulus ratio (fibreglass sheet: VPPMC strip) on the snap-through characteristics. Experimental results and FE simulation show good agreement with regard to snap-through behaviour of the bistable structure and from this, the bistability mechanisms are discussed.

*Keywords:* A. Polymer-matrix composites (PMCs); B. Residual/internal stress; C. Finite element analysis (FEA); D. Mechanical testing; Bistable (snap-through) structure.

---

\* Corresponding author. Tel.: + 44 1482 465071; fax: +44 1482 466664.  
*E-mail address:* k.s.fancey@hull.ac.uk (K.S. Fancey).

## 1. Introduction

Morphing technology has received increasing interest in recent years for applications involving aircraft aerofoils [1-3], automobile structures [4], and wind turbine blades [5]. This arises from the potential benefits that morphing structures can provide over the more conventional mechanical approaches; i.e. in terms of reduced cost, complexity and weight, combined with improved aerodynamic efficiency and shape adaptivity. Morphing structures generated from utilising the deformation of fibre-reinforced polymeric matrix composites (PMCs) have been developed since the 1980s [6-8]. These can be bistable or multistable structures, which possess the ability to change rapidly or 'snap-through' from one stable shape to another by external stimulation, e.g. from piezoelectric patches [9], piezocomposite actuators [10] or pressure [11,12]. To date, these morphing (shape-adaptive or shape-changing) structures are generally produced through: (i) thermally induced residual stresses in unsymmetric laminates or (ii) elastically induced compressive stresses in symmetric laminates.

For (i), research has been carried out by many investigators [6-8, 13-19], in which the mismatch in thermal expansion coefficients between the reinforcing fibre and matrix materials is exploited. The resulting residual stresses developed during cool-down from curing can generate large out-of-plane displacements to give bistable or multistable behaviour [6, 7]. There is however, evidence to show that the residual stresses generated from thermal expansion mismatch within a non-symmetrical multi-layer laminate are highly susceptible to hygrothermal variability [15, 17, 20-22]. Thus it is difficult to exploit thermal effects [23].

For (ii), the concept of morphing structures from symmetric laminates is comparatively recent. Initial studies focused on exploiting thermal stresses between different fibre prepreg materials, i.e. 90° carbon fibre laminated with 0° unidirectional glass fibre, to produce a multistable structure with symmetric layup across the mid-plane [24]. Nevertheless, Tuttle [25] demonstrated that the thermal residual stresses within a composite could be reduced or converted into compressive strains by adopting elastic fibre prestressing. Daynes et al [11, 26] utilised the principle to produce morphing symmetric laminates. By applying prestrain to the 0° fibre layers for both CFRP and GFRP [0/90/90/0] laminates during resin curing, it was found that bistability could be achieved [11]. In further work [26], prestressing was applied to selected fibre layers during curing: here, bistability was produced from laminate layups of  $[0^P/90/90^P/0]_T$  and  $[0^P/90/90/90^P/90^P/0]_T$ , with superscript <sup>P</sup> referring to prestressing in fibres. In addition

to morphing laminates, Lachenal et al [27] produced a bistable twisting I-beam by combining two elastically prestressed CFRP flanges on GFRP web geometry, the prestress being achieved by flattening the flanges previously moulded to a curved configuration. By applying an external moment, the beam could snap between two stable shapes. Similar twisting structures, that had multistable capability, were also developed [28, 29].

Although the use of elastically generated fibre prestress offers significant advantages over thermally induced stress for morphing structures, there are potential drawbacks. First, fibre length, orientation and spatial distribution are restricted by the need to apply fibre elastic tension as the matrix cures [30]; these restrictions can compromise fibre and mould geometries for more complex structural situations. Also, achieving suitable stretching rig and reliable fibre clamping designs can be technically challenging [26, 31]. Second, the matrix material is polymeric; thus localised matrix creep at the fibre-matrix interface regions within the composite may occur, in response to the elastically generated prestress. This can be expected to cause some deterioration in prestress levels [30] as recently demonstrated by Mostafa et al [32].

Viscoelastically prestressed polymeric matrix composites (VPPMCs) offer a novel solution to morphing composite production. To produce a VPPMC, polymeric fibres are subjected to tensile creep so that they progressively extend through viscoelastic deformation; the creep load is then released before the fibres are moulded into a matrix. Following matrix curing, the previously strained fibres continue to attempt viscoelastic recovery within the solidified matrix. This results in compressive stresses being generated within the matrix, and these are counterbalanced by residual tension in the fibres. Previous work has demonstrated notable improvements in mechanical properties from VPPMCs, especially in terms of impact toughness and flexural stiffness, using nylon 6,6 fibres [30, 33, 34] and UHMWPE fibres [35, 36]. There are significant opportunities offered by VPPMC processing, as the fibre stretching and moulding operations are decoupled. Recent published work has also shown that the viscoelastic fibre stretching period can be significantly reduced from 24 h to tens of minutes, by using higher creep stress levels [37]. In addition to simplifying equipment requirements and procedures, there is total flexibility in terms of product geometry [38]. A further benefit is longevity: any potential for deterioration through localised matrix creep would be offset by activity from longer term viscoelastic recovery mechanisms within the polymeric fibres [30]. Although viscoelastic activity is temperature sensitive, recent accelerated ageing (time-temperature superposition) experiments on nylon 6,6 fibre-based VPPMCs have

demonstrated no deterioration in impact performance over a duration equivalent to ~25 years at 50°C [33].

Clearly, the benefits from VPPMC technology could be applicable to morphing structures. The initial development of a mechanically bistable morphing composite structure, based on the use of viscoelastically generated prestress, has been recently reported [39], and subsequently presented in conference proceedings [40]. This paper provides further details on the fabrication and evaluation of the bistable structure. Snap-through behaviour was investigated through both experimental and finite element (FE) analysis. The purpose of an FE model was to evaluate the nonlinear response from snap-through of the bistable assembly, and offer further insight into the mechanisms of bistability.

## 2. Background

### 2.1. Bistability principles

To create a simple bistable structure, four identical VPPMC strips can be bonded to a thin, flexible resin-impregnated fibreglass sheet, as shown schematically in Fig. 1. The cross-sectional spatial density of fibres (such as nylon 6,6) used for producing the prestress in a VPPMC strip is normally non-uniform, due to the use of open casting. This arises from fibres settling towards the bottom of the mould prior to curing taking place [30, 33, 34]. As described by Timoshenko [41], the critical load  $P_{cl}$  for the generation of elastic buckling (beam bending) from an eccentrically compressed strut can be calculated through Euler's formula:

$$P_{cl} = \frac{\pi^2 EI}{4L^2} \quad (1)$$

where  $E$  is the Young's modulus and  $L$  is the beam length;  $I$  is the second moment of area, which is  $(bh^3/12)$  for a rectangular beam of width  $b$  and thickness  $h$ . Therefore, beyond the critical compressive load, the resulting non-uniform stress distribution created through the thickness of a thin flat strip can be expected to cause bending, to give a mid-span deflection,  $\delta$ , in Fig. 1. If a VPPMC strip is considered in isolation,  $\delta$  can be associated with the prestressed beam relationship [42]:

$$\delta = \frac{PeL^2}{8E_m I} \quad (2)$$

Here,  $P$  is the force generated from the compressive prestress and  $E_m$  is the elastic modulus of the matrix material;  $I$  and  $L$  are as defined in Eq. (1). The distance between beam and fibre centroids,  $e$ , can be estimated from the cross-sectional spatial density of fibres in a composite strip sample. As shown in Fig. 1, the upper and lower strips are oriented to deflect in opposite directions, giving opposing cylindrical configurations within the structure. Therefore, the whole assembly should be capable of demonstrating bistability.

For a situation where a simple concrete beam is prestressed by steel rods which occupy a relatively small proportion of the total beam volume, Eq. (2) can be expected to give realistic predictions [43]. For the current work however, the assumption that  $E_m$  in Eq. (2) can be represented by the matrix modulus alone may be unrealistic. This arises from (i) the nylon fibres occupying a significant proportion of the total beam volume and (ii) the addition of the resin-impregnated fibreglass sheet. The limitations and applicability of Eq. (2) on beam structure configurations relating to the bistable composite assembly have been previously discussed [40]. In this work however, such limitations have been addressed through the use of FE-based numerical simulation as described below.

## 2.2. *The finite element method*

FE analysis offers an approximate solution to realistic types of structures. To understand further the deformation mechanisms of the VPPMC-based bistable morphing composite structure, it is necessary to apply FE to the nonlinear response from snap-through and determine the equilibrium configurations. Thus, FE modelling was used to complement the experimental study by offering further insight into the snap-through mechanisms from bistability.

The simulation of viscoelastic prestress was achieved through a predefined temperature change in the fibre material. During cool down from high temperature curing in composite production, it is well known that residual thermal stresses will be generated due to mismatch in thermal expansion coefficients between the constituent materials [31, 44, 45]. Therefore, in an FE model, the force can be generated by employing a temperature change to the embedded fibre material, with a constant thermal expansion

coefficient [26, 46]. Since recovery force inside a VPPMC sample has been measured through experimental procedures [47], the magnitude of the recovery force can be represented by the thermally induced force within a model, to give deflection,  $\delta$ , as shown in Fig. 1. Detailed construction of the FE model is presented in Section 4.

### 3. Experimental procedures

#### 3.1. Production of VPPMC strips

Production of the VPPMC strips followed previously described procedures [30, 33, 34] and the main points are outlined here. A continuous multifilament yarn of nylon 6,6 fibres with 140 filaments, 26  $\mu\text{m}$  filament diameter and 94 tex, was used. This was supplied by Ogden Fibres Ltd, UK. The yarn was annealed at 150°C in a fan-assisted oven for 0.5 h; this step was essential for providing long-term viscoelastic recovery following the applied creep load. As ~330 MPa has been the most commonly used stress for VPPMC production [30, 33, 34, 38, 47-49], the yarn was then subjected to a 330 MPa tensile creep stress for 24 h under ambient conditions (20-21°C, 30-40% RH). The creep load was subsequently released and the yarn was folded, cut into lengths of ~500 mm and brushed into flat ribbons ready for moulding.

The matrix material was a clear-casting polyester resin, Reichhold PolyLite 32032, mixed with 2% MEKP catalyst, supplied by MB Fibreglass, UK. This had a gel-time (at room temperature) of ~0.3 h. Unidirectional continuous fibre composites were open-cast in two aluminium moulds, the process being completed within 0.5 h following the fibre stretching procedure. Each mould had a polished channel that was 10 mm in width and 1 mm in depth, for casting a 460 mm strip of material. The average (macroscopic) fibre volume fraction was ~18%. The two composite strips were then removed from the moulds after ~2 h and each strip was cut into two 200 mm lengths to provide the four separate VPPMC strips.

#### 3.2. Production of the bistable composite structure

To produce a bistable composite assembly, a 200 × 200 mm square fibreglass tissue, with an areal density of 30  $\text{gm}^{-2}$  was used. First, the tissue was impregnated, by hand lay-up, with the same resin

used in Section 3.1. Following resin curing, after ~24 h, two of the 200 mm VPPMC strips were bonded to each side of the fibreglass layer. The assembled composite sample was then held under a weighted solid plate for a further 48 h. For repeatability purposes, three of these VPPMC-based ‘test’ samples were produced and stored at 20-21°C for subsequent evaluation. As facilities were limited to producing one sample at a time, there was some variation in sample age on subsequent testing.

A ‘control’ sample of the composite assembly was also required, this being structurally identical to the VPPMC-based test samples, but with the 24 h fibre stretching stage omitted. Instead, the annealed yarn at this stage of production was stored under the same ambient conditions for 24 h, prior to composite production. Therefore, the control sample provided a reference to determine whether other production-based stresses might be significant.

The fibreglass layer, during its production, was placed on mould release film. Therefore, the side in contact with the film surface had a smooth finish while the opposite side had a comparatively rough surface. To clarify any potential influences from this slight difference, cylindrical shapes with the smooth resin layer on the outside convex surface were denoted as Shape I; while those with the smooth layer on the inside concave surface were denoted as Shape II.

### 3.3. *Evaluation of the bistable composite assembly*

The three test assemblies were evaluated for static (stable) deflection at the centre of each VPPMC strip, this being associated with  $\delta$  in Fig. 1 and Eq. (2). Subsequently, a Lloyd Instruments EZ-50 testing machine with a 2.5 N load cell was used for dynamic (snap-through) evaluation of the bistable samples. Each test sample was supported on a rigid three-point bending jig as illustrated in Fig. 2, and a jig span of 190 mm enabled the supports to be centred on the VPPMC strips at the sample edges. Bending was achieved through a point-force indenter as shown schematically in Fig. 2. The three bistable samples were each tested three times to give a total of nine readings in each snap-through direction with a test speed of 60 mm/min. As explained in Section 3.2, there was some variation in sample age for the snap-through tests (i.e. 338, 434, 646 h), thus the average age for evaluation of snap-through behaviour was considered to be ~500 h after production.

## 4. **FE model**

#### 4.1. Material properties required for the FE model

To construct the FE model, certain geometrical information and material properties relating to the bistable structure were required. For geometry, isolated VPPMC strips were produced following the procedures described in Section 3.1, to evaluate the dimensions of a single beam structure. Here, the resulting mean values based on four samples were  $9.89 \pm 0.01$  mm in width and  $1.10 \pm 0.02$  mm in thickness. A further batch of four cured fibreglass strips were made following Section 3.2 but with dimensions of  $200 \times 10$  mm. This enabled the thickness of the mid-layer within a bistable assembly to be determined, and the mean value was  $0.40 \pm 0.03$  mm. The glass fibre volume fraction was found to be 3.2%, based on weight measurements.

Table 1 Mechanical properties of the materials used in the bistable assembly.

	Nylon 6,6 fibre [50]	Polyester resin [34, 51]	E-glass fibre fabric [52]
Density, $\rho$ (g/cm <sup>3</sup> )	1.14	1.12	2.55
Young's modulus, $E$ (GPa)	3.3	3.3	72
Poisson's ratio, $\nu$	0.41	0.40	0.25
Thermal expansion coefficient, $\alpha$ (°C <sup>-1</sup> )	$90 \times 10^{-6}$	--	--

The required mechanical properties of the materials involved are listed in Table 1. As explained in Section 2.2, the thermal expansion coefficient of nylon fibre was needed for the model to induce fibre prestressing through a predefined temperature change. Another concern was the effective modulus of the glass fibre mid-layer. Since this layer was very thin (~0.4 mm), measurement of the elastic modulus through three-point bending tests [34] was unrealistic. Thus a theoretically-based predictive model was considered to determine the stiffness of the mid-layer. It is well-known that for a two-phase composite with known fibre volume fraction ( $V_f$ ), the simplest model to predict the effective modulus is the 'rule of mixtures', which is represented by the Voigt-Reuss (VR) bounds [53-55]. The Voigt upper bound is the isostrain rule of mixtures, which assumes the fibre reinforcement and matrix are arranged in parallel and subject to the same stress. The Reuss lower bound is the isostress rule of mixtures, in which the applied stress is perpendicular to the fibres and constituents of the composite undergo the same stress. The upper bound  $E_{VR}^u$  and lower bound  $E_{VR}^l$  can be represented through:

$$E_{VR}^u = E_f V_f + E_m V_m \quad (3)$$

$$E_{VR}^l = \left[ \frac{V_f}{E_f} + \frac{V_m}{E_m} \right]^{-1} \quad (4)$$

where  $E_f$  is the elastic modulus of the fibre reinforcement;  $V_m$  is the matrix volume fraction; the superscripts 'u' and 'l' correspond to the upper and lower bounds, respectively.

For randomly oriented two phase fibre composites, an expression similar to the rule of mixtures for the effective modulus  $E_{RC}$  can be utilised as follows [56]:

$$E_{RC} = k E_f V_f + E_m V_m \quad (5)$$

where  $k$  is a fibre efficiency parameter, which depends on  $V_f$  and the  $E_f/E_m$  ratio; the latter is usually between 0.1 to 0.6. For a two-dimensional (in plane) random orientation of fibres, it has been demonstrated that  $k$  is 3/8 [56]. Thus for our work, the suitability of Eq. (5) to predict  $E_{RC}$  for glass fibre mat reinforced PMCs was required. With the material properties listed in Table 1, the  $E_{RC}$  is plotted in Fig. 3 as a function of  $V_f$ , together with the upper and lower VR bounds from Eqs. (3) and (4). Good agreement is found between predicted values from Eq. 5 with  $k = 3/8$  and experimental points from published work [57, 58]. Thus Eq. (5) enables the effective modulus of the mid fibreglass layer ( $V_f = 3.2\%$ ) in our sample to be calculated (with  $k = 3/8$ ). This gives a value of 4.06 GPa.

#### 4.2. FE model construction

For the FE study, ABAQUS software was adopted. Numerical simulation analysis was developed to identify the structural response of the bistable assembly and the possible effects of various factors on the sample configuration. To simulate the bistable morphing structure as illustrated in Fig. 1, the model consisted of four identical  $200 \times 10 \times 1$  mm strips with 18%  $V_f$  and a  $200 \times 200 \times 0.4$  mm fibreglass layer (Section 4.1). As fibres settle towards the bottom of the mould (Section 2.1), fibres in the

model were set to be 0.2 mm away from the beam centroids, and constrained within the matrix utilising the ‘embedded region’ method; this value has been verified through optical microscopy [39]. Strips were then bonded on the edges of the fibreglass layer through ‘tie’ constraints and numbered as ‘X1’, ‘X2’, ‘Y1’, ‘Y2’, with strips ‘X1’ and ‘X2’ placed on the Z- side of the mid-layer, and strips ‘Y1’, ‘Y2’ on the Z+ side, as presented in Fig. 4.

The analysis was performed using the following: T3D2 elements (a 2-node linear 3-D truss) on fibres, C3D8R elements (an 8-node linear brick, reduced integration, hourglass control) on VPPMC strips, and S4R elements (4-node general purpose reduced integration shell elements) on the mid-layer. Geometrically nonlinear algorithms ‘NLGEOM’ were employed. The ‘stabilize’ function was used in the model to minimise the instabilities [11, 59] with a damping factor of  $1 \times 10^{-6}$ . Element size used for the mid-layer was  $5 \times 5$  mm, and  $5 \times 1 \times 0.2$  mm on the strips, which gave a total element number of 9600. The snap-through model developed in this work comprised three steps:

Step-1: Generation of the prestress within a composite strip;

Step-2: Snap-through response of the bistable structure upon loading;

Step-3: Recovery of the structure after loading.

In Step-1, since recovery force within a VPPMC sample can be measured experimentally [47], a particular viscoelastic recovery force may be represented through the cooling of a polymeric fibre as explained in Section 2.2. As fibres are constrained within the composite, compressive stresses in the matrix are generated through the fibre-matrix interface. Since the peak curing temperature of the resin used in this study was found to be less than  $28^\circ\text{C}$  [60], any residual thermal stresses induced by resin curing could be neglected in the FE analysis. Step-2 was achieved through applying displacement to an indenter with 6 mm radius, to simulate the point-force indenter in Fig. 2, at a velocity of 60 mm/min. ‘Analytical rigid’ was employed to simulate the indenter. This did not require meshes, so it could reduce the simulation period and minimise the mesh dependent snap-through load [61]. In Step-3, the loading was removed to enable the model to recover freely.

The constrained translational degrees of freedom applied to the plate in different steps are shown in Fig. 4; no rotational constraints were applied to the panel. Numerical simulation results were compared with the experimental data to determine model significance, i.e. the experimental snap-through process of the bistable assembly with sample age of  $\sim 500$  h, loaded with the point-force indenter (Section 3.3) at 60 mm/min was chosen as the reference. Development of the snap-through process and effect of

modulus ratio on snap-through behaviour were subsequently performed, based on the adjusted model solution. The results were then analysed to establish the snap-through mechanism for the proposed bistable structure.

## 5. Results and discussion

### 5.1. Static evaluation of the bistable structure

Fig. 5 shows a typical VPPMC-based test (bistable) sample in comparison with the control sample. The test sample with curved surface is shown in one of the two stable shapes, i.e. Shape II as described in Section 3.2. It is clear that the control sample is flat, signifying that there were no other production-based residual stresses of any significance. Therefore it may be concluded that deflection from the test sample is generated through viscoelastic prestress alone. The static deflection  $\delta$  (as shown in Fig. 5) was measured with time, and the mean from all three samples at  $\sim 500$  h was found to be  $11.6 \pm 0.4$  mm standard error. This was based on 6 readings, i.e. one reading from each stable state.

### 5.2. Dynamic (snap-through) characteristics

Fig. 6 shows representative load-displacement curves from a typical bistable sample tested at 60 mm/min. The snap-through direction for (a) is Shape I to Shape II, while (b) represents the snap-back process from Shape II to Shape I. The snap-through process in both directions initially shows a region of fluctuation below  $\sim 3$ mm displacement, followed by a critical snap-through load. These initial fluctuations can be attributed to the snap-through effect from localised ripples on the sample surface as highlighted in Fig. 7. A possible explanation for the fluctuation effect arises from the bistable assembly being produced through the hand lay-up process (Section 3.2). Thus some non-uniformity in the distribution of resin and variability in areal density of the glass fibre sheet throughout the mid-layer can be expected, resulting in a variation in load-displacement characteristics for the localised ripples. Moreover, although the indenter was positioned at the centre of the assembly, the sample was not geometrically perfect; thus displacement effects from the point loading force could propagate preferentially in any direction.

Table 2 Point-force loading snap-through test results with a test speed of 60 mm/min; SE is the standard error of the mean.

Sample No.	Test speed 60 mm/min	
	Peak load (N)	Displacement at peak load (mm)
1	$1.32 \pm 0.02$	$16.0 \pm 0.4$
	$1.26 \pm 0.02$	$13.1 \pm 0.2$
2	$1.10 \pm 0.04$	$17.5 \pm 0.8$
	$1.47 \pm 0.01$	$17.6 \pm 0.5$
3	$1.24 \pm 0.03$	$14.1 \pm 0.1$
	$1.57 \pm 0.08$	$17.7 \pm 0.2$
Mean $\pm$ SE	$1.32 \pm 0.04$	$16.0 \pm 0.5$

The results of peak loading force and corresponding displacement from the snap-through tests are listed in Table 2. At a sample age of  $\sim 500$  h, the peak force and displacement were found to be  $1.32 \pm 0.04$  N and  $16.0 \pm 0.5$  mm; the deviations in data values may be attributed to variations arising from sample age and hand lay-up processing. Clearly, the displacement values in Table 2 are larger than the static values ( $11.6 \pm 0.4$  mm) reported in Section 5.1. Since displacement recorded during snap-through was the maximum value from the centre of each sample, the differences may be explained by flexibility effects within the fibreglass sheet, as the static values were measured at the edges of each sample.

### 5.3. FE analysis

#### 5.3.1. Numerical simulation

The loading history for FE analysis is illustrated in Fig. 8. As explained in Section 4.2, prestress was introduced to the composite through a 'predefined field' in Step-1, and only fibres were subjected to the temperature change  $\Delta T$ . As the amplitude of  $\Delta T$  determines the force that is generated, which leads to sample deflection, a linear relationship was obtained from the FE model, which could predict the  $\Delta T$  value for the required deflection at  $\sim 500$  h; i.e. 11.6 mm. The relationship ( $\delta = 0.0973 \Delta T + 0.3941$ ) gave a value of  $115^\circ\text{C}$  for  $\Delta T$ .

Using the parameters outlined above and information from Section 4, the FE model was generated and the first stable shape in the y-direction after Step-1 is shown in Fig. 9. This is associated with the von Mises stress distribution within the mid-fibreglass layer. Since the stress within the fibres is much higher than the strip and layer, the stress distribution is not clearly presented in Fig. 9 (a). Thus the mid-layer is isolated to demonstrate the stress distribution as shown in Fig. 9 (b). It shows that the von

Mises stress is symmetrical about the centre of the structure, and the maximum von Mises stress is located within the area influenced by the combined effect of the strips. As the stable cylindrical shape is in the  $y$ -direction, any deflection in the  $y$ -direction is not constrained, thus a low stress distribution area is formed along this direction. The strip deflection in the  $x$ -direction however, is constrained by the structure, which therefore gives a higher concentration of stress.

Step-2 and Step-3, as described in Section 4.2 and Fig. 8, were then applied to the FE model. In contrast with the experimental investigation, the model is based on homogeneous materials, the whole structure is perfectly symmetrical, and snap-through and snap-back processes are identical. Therefore, only the snap-through process was investigated and the stable shapes before and after loading are shown in Fig. 10. Note that the white object represents the simulated rigid point-force indenter, and the deflection of the second stable shape in the  $x$ -direction is found to be equal to that of the first stable shape, i.e. 11.6 mm. The loading velocity of 60 mm/min for Step-2 enables direct comparison of the FE results to the experimental snap-through process in Section 5.2, as shown in Fig. 11.

As discussed in Section 5.2, the region of fluctuation at the beginning of the experimental loading process was thought to be caused by variations resulting from sample production, while the FE model was based on homogenous materials and uniform geometries. Therefore, the FE load shows a linear relationship with loading displacement, as demonstrated in Fig. 11. The FE model gave a peak load of 1.26 N which is comparable to the experimental data of  $1.32 \pm 0.04$  N, and the variation could be attributed to optimisation of model geometry (Section 4.2); however, the displacement at peak load was 8.42 mm, i.e. approximately half the value obtained from experimental data ( $16.0 \pm 0.5$  mm). For displacements above  $\sim 8$  mm, the gradient of the experimental curves prior to snap-through is similar to the FE curve. Therefore, we suggest that the discrepancy below 8 mm may be attributed to displacement losses from fluctuations below 3 mm in the former case (Section 5.2); hence the shift in peak load position. It can also be seen that the load-displacement process in the numerical simulation differs from the experimental characteristic in terms of snap-through behaviour: in the experimental process, the snap-through occurs rapidly when peak force is reached; in the FE simulation however, there is some delay after reaching the peak load. Furthermore, it was found that the critical displacement value in Step-2 for the snap-through phenomenon to occur in the model was 14.2 mm, i.e. similar to the displacement at peak load from the experimental results. When this value was reached, the panel deformed quickly to the second stable shape. Thus, it can be concluded that since the actual sample is not perfectly symmetrical,

snap through occurs when it has reached the peak load, while the FE results show that peak load and indenter displacement are both essential to the snap-through behaviour.

The FE model of the morphing bistable structure demonstrates validity in terms of peak load and critical displacement. Despite the differences outlined above, it is clearly a convenient tool to investigate factors that could affect bistable snap-through behaviour. These include prestress level  $P$ , fibre volume fraction  $V_f$ , edge length  $L$ , and modulus of the mid-layer  $E_{ML}$ . Of particular interest are the effects of sample deflection and material modulus values on the development of bistable behaviour and understanding of the underlying mechanisms. To investigate the effects of various factors, the basic model parameters are maintained constant, and the chosen factor can then set as the variable.

### 5.3.2. *Development of bistable behaviour*

It has been experimentally demonstrated that the bistable sample deflection  $\delta$  is directly proportional to prestress force  $P$  in Eq. (2) [40]. Since sample deflection  $\delta$  is proportional to  $\Delta T$  (Section 5.3.1), FE analysis can be used to investigate the development of snap-through behaviour in terms of model deflection; i.e. realistic deflections can be achieved through adjusting the prestress levels and  $V_f$  within a composite. The snap-through responses of the panel with  $\delta$  ranging from 1.6 to 11.7 mm were investigated using the FE method and results are shown in Fig. 12. Here, the dashed lines represent the trends in maximum load and critical indenter displacement. Inserted figures show the corresponding deformation (contours) during different snap-through stages.

As shown in Fig. 12, pre-snap-through behaviour basically follows the same characteristic, and the maximum (peak) load increases with deflection. No clear critical snap-through indenter displacement is observed with sample deflections less than 3.7 mm and, beyond 5.8 mm, the load at critical displacement increases linearly with deflection. Furthermore, with increasing deflection, peak load and critical displacement diverge from each other, and gradually form two snap-through features as highlighted by the images in Fig. 12. Feature 1 is formed as contours in the  $y$ -direction contribute collectively to snap, giving a peak load to the curve. Feature 2 corresponds to a similar effect in the  $x$ -direction and occurs when the loading indenter reaches the critical displacement; the structure then jumps rapidly into the second stable shape.

### 5.3.3. Effect of modulus ratio

Section 5.3.2 demonstrates that the snap-through behaviour of the proposed bistable structure depends on the movement of contours in both  $x$ - and  $y$ -directions. As model deflections increase, there is greater divergence between peak load and critical displacement, which is detrimental to a rapid snap-through response. This section looks into the feasibility of improving this response. The sample stiffness could be considered as a vital factor in affecting the snap-through behaviour, especially since the VPPMC strips and mid-layer were different materials (Sections 3.1 and 3.2). Thus a modulus ratio,  $R_E$ , can be defined as ( $E_{\text{layer}}/E_{\text{strip}}$ ); i.e. the ratio of elastic moduli between the mid-layer and prestressed strips. Therefore, the FE model developed in Section 5.3.1 is denoted with an  $R_E$  value of (4.06/3.30), i.e. 1.23.

To investigate the modulus ratio effect, model parameters from Section 5.3.1 were adopted. With  $R_E$  as the variable, the corresponding snap-through responses are plotted in Fig. 13. Here, the dashed line shows how the maximum load during snap-through varies with  $R_E$ . Thus when the mid-layer is more flexible than the VPPMC strips (i.e.  $R_E < 1$ ), a large snap-through region is developed; conversely, as  $R_E$  increases, (the layer becoming stiffer), the two features (as highlighted in Fig. 12) gradually merge into one peak. The maximum load can be seen to reach a peak at an  $R_E$  value of 4, and then starts to decrease. Therefore, the ability of the bistable structure to respond rapidly can be enhanced through adjustment of the  $R_E$  value; i.e. material properties can be tailored to produce bistable structures for specific objectives.

Fig. 14 shows the effect of  $R_E$  on maximum load, critical displacement and model deflection. Here, the maximum load peaks at an  $R_E$  value of 4, concurring with Fig. 13. The critical displacement for snap-through and model deflection both decrease as the mid-layer stiffness increases, becoming closer, thus facilitating a more rapidly responding snap-through.

### 5.3.4. Bistability mechanisms

The snap-through behaviour of a bistable structure utilising VPPMC technology has been investigated through both experimental and numerical methods. For a symmetrical model consisting of homogeneous materials, the snap-through performance is dependent on the contours accumulated in two directions during the loading process, which leads to two snap-through features: (i) the first contour

transition generates a peak in the load-displacement curves; (ii) the following contour transition determines the critical displacement in the snap-through behaviour. As the structure is based on two composite materials, a critical value of modulus ratio exists, where the two features merge into one snap-through peak (Section 5.3.3). This infers that the rapid response characteristics of the bistable structure can be improved through tailoring the material properties. The differences between numerical and experimental results illustrated in Fig. 11 may be further explained: since the real sample is not perfectly homogeneous as demonstrated in Fig. 7 (localised ripple effect), the first contour effect, i.e. Feature 1 (as observed in the model), could be dispersed into small ripples during loading, which leads to its disappearance. Displacements from the small ripples occur at an early stage of loading to create the area of fluctuation as shown in Fig. 6, and this we believe, shifts the critical snap-through displacement, as demonstrated in Fig. 11.

#### 5.3.5. *Future considerations*

Since composite materials can reduce structural weight and complexity, their use as morphing structures adds an extra dimension to their exploitation within engineering applications. In aerospace, simple aerofoil shape control can be achieved by using shape-adaptive structures [1-3]. For automotive applications, there is interest in shape-changing structures for improved aerodynamic performance [4]. Moreover, morphing structures in wind turbines offer new approaches for load control to reduce blade stress [5]. Clearly, progression from the development of bistable to multistable composite structures will enable improved control and increased shape-changing variability, thereby facilitating further exploitation.

In this paper, we have presented an alternative solution to producing bistable morphing composite structures. As highlighted in Section 1, the viscoelastic fibre prestressing technique offers benefits in terms of flexibility in manufacture and moulding geometry, with demonstrable product longevity. Multistable structures may also be achievable, based on viscoelastically generated prestress. For example, single bistable structures could be combined to produce a multistable assembly. Here, FE analysis based on further development of the current model would facilitate this work, as it should lead to optimised model solutions for more efficient experimental verification.

## 6. Conclusions

This work reports the snap-through behaviour of a novel morphing bistable structure, based on the principles of viscoelastically generated prestress. An FE model was successfully developed to simulate the bistability, and the viscoelastic recovery mechanism within a VPPMC was achieved by exploiting thermally induced dimensional changes within the fibre material. The main findings are:

- (i) A localised ripple effect was observed during snap-through testing of the bistable structure with a point-force indenter, which was not predicted through numerical simulation. This discrepancy is attributed to the non-uniform distribution of resin and glass fibre within the mid-layer, resulting in unstable load transfer.
- (ii) Numerical simulation results of the snap-through behaviour show good agreement with the experimental work in terms of peak load and critical displacement. Investigation into the development of bistable behaviour shows the contours accumulated in both  $x$ - and  $y$ -directions give two features which determine the snap-through performance of the bistable structure. These two features gradually diverge as model deflections increase.
- (iii) By considering the modulus ratio effect, the model solution demonstrates that rapid response from the bistable structure can be improved through adjustment of the modulus ratio value; in practice, this can be achieved through tailoring the material properties.
- (iv) From the experimental and numerical simulation results, analysis of the bistable behaviour offers further insight into the snap-through mechanisms (critical load and displacement) of these structures.

VPPMC technology offers a novel solution to produce morphing composite structures. It provides flexibility in terms of product geometry and offers product longevity. Moreover, the influence of sample deflection and modulus ratio show that VPPMC-based morphing composite structures could be tailored to various industrial applications.

## Acknowledgements

Two of the authors (B.W. and C.G.) would like to thank the financial support from the China Scholarship Council (CSC). A PhD degree fee waiver from the School of Engineering for one of the

authors (B.W.) is also gratefully acknowledged. Special thanks go to Garry Robinson and Tung Lik Lee from the School of Engineering for their technical support.

ACCEPTED MANUSCRIPT

## References

- [1] Barbarino S, Bilgen O, Ajaj RM, Friswell MI, Inman DJ. A review of morphing aircraft. *J Intel Mat Syst Str* 2011; 22(9):823-77.
- [2] Thill C, Etches J, Bond I, Potter K, Weaver PM. Morphing skins. *Aeronaut J* 2008; 112(1129):117-39.
- [3] Sofla AYN, Meguid SA, Tan KT, Yeo WK. Shape morphing of aircraft wing: Status and challenges. *Mater Design* 2010; 31(3):1284-92.
- [4] Daynes S, Weaver PM. Review of shape-morphing automobile structures: concepts and outlook. *Proceedings of the Institution of Mechanical Engineers, Part D: Journal of Automobile Engineering* 2013; 227(11):1603-22.
- [5] Lachenal X, Daynes S, Weaver PM. Review of morphing concepts and materials for wind turbine blade applications. *Wind Energy* 2013; 16(2):283-307.
- [6] Hyer MW. The Room-Temperature Shapes of Four-Layer Unsymmetric Cross-Ply Laminates. *J Compos Mater* 1982; 16(4):318-40.
- [7] Hyer MW. Some observations on the cured shape of thin unsymmetric laminates. *J Compos Mater* 1981; 15(2):175-94.
- [8] Hyer MW. Calculation of the room-temperature shapes of unsymmetric laminates. *J Compos Mater* 1981; 15:296-310.
- [9] Portela P, Camanho P, Weaver PM, Bond I. Analysis of morphing, multi stable structures actuated by piezoelectric patches. *Comput Struct* 2008; 86(3-5):347-56.
- [10] Flatau AB, Schultz MR. A new concept for active bistable twisting structures. *Smart Mater Struct* 2005; 5764:241-52.
- [11] Daynes S, Potter KD, Weaver PM. Bistable prestressed buckled laminates. *Compos Sci Technol* 2008; 68(15-16): 3431-7.
- [12] Daynes S, Weaver PM. Analysis of unsymmetric CFRP–metal hybrid laminates for use in adaptive structures. *Compos Part A* 2010; 41(11):1712-18.
- [13] Bowen CR, Betts DN, Giddings PF, Salo AIT, Kim HA. A study of bistable laminates of generic lay-up for adaptive structures. *Strain* 2012; 48(3):235-40.
- [14] Gude, M., W. Hufenbach, and C. Kirvel. Piezoelectrically driven morphing structures based on bistable unsymmetric laminates. *Compos Struct*, 2011; 93(2):377-82.
- [15] Hufenbach W, Gude M. Analysis and optimisation of multistable composites under residual stresses. *Compos Struct* 2002; 55(3):319-27.
- [16] Betts D. Modelling and optimisation of bistable composite laminates. PhD Thesis. University of Bath: United Kingdom; 2012.
- [17] Gigliotti M, Wisnom MR, Potter KD. Loss of bifurcation and multiple shapes of thin [0/90] unsymmetric composite plates subject to thermal stress. *Compos Sci Technol* 2004; 64(1):109-28.
- [18] Dano ML, Hyer MW. Thermally-induced deformation behavior of unsymmetric laminates. *Int J Solids Struct* 1998; 35(17):2101-20.
- [19] Akira H, Hye MW. Non-linear temperature-curvature relationships for unsymmetric graphite-epoxy laminates. *Int J Solids Struct* 1987; 23(7):919-35.

- [20] Gigliotti M, Wisnom MR, Potter KD. Development of curvature during the cure of AS4/8552 [0/90] unsymmetric composite plates. *Compos Sci Technol* 2003; 63(2):187-97.
- [21] Etches J, Potter K, Weaver PM, Bond I. Environmental effects on thermally induced multistability in unsymmetric composite laminates. *Compos Part A* 2009; 40(8):1240-47.
- [22] Gigliotti M, Minervino M, Grandidier JC, Lafarie-Frenot MC. Predicting loss of bifurcation behaviour of 0/90 unsymmetric composite plates subjected to environmental loads. *Compos Struct* 2012; 94(9):2793-808.
- [23] Daynes S, Weaver PM. Stiffness tailoring using prestress in adaptive composite structures. *Compos Struct* 2013; 106:282-87.
- [24] Potter KD, Weaver PM. A concept for the generation of out-of-plane distortion from tailored FRP laminates. *Compos Part A* 2004; 35(12): 1353-61.
- [25] Tuttle ME. A mechanical/thermal analysis of prestressed composite laminates. *J Compos Mater* 1988; 22(8): 780-92.
- [26] Daynes S, Diaconu CG, Potter KD, Weaver PM. Bistable Prestressed Symmetric Laminates. *J Compos Mater* 2010; 44(9):1119-37.
- [27] Lachenal X, Daynes S, Weaver PM. A non-linear stiffness composite twisting I-beam. *J Intel Mat Syst Str* 2013; 25:744-54.
- [28] Lachenal X, Weaver PM, Daynes S. Multi-stable composite twisting structure for morphing applications. *P Roy Soc A-Math Phy* 2012; 468(214): 1230-51.
- [29] Lachenal X, Weaver PM, Daynes S. Influence of transverse curvature on the stability of prestressed helical structures. *Int J Solids Struct* 2014; 51(13):2479-90.
- [30] Fancey KS. Fiber-reinforced polymeric composites with viscoelastically induced prestress. *J Adv Mater* 2005; 37(2):21-9.
- [31] Krishnamurthy S. Pre-stressed advanced fibre reinforced composites fabrication and mechanical performance. PhD Thesis. Cranfield University: United Kingdom; 2006.
- [32] Mostafa NH, Ismarrubie ZN, Sapuan SM, Sultan MTH. The influence of equi-biaxially fabric prestressing on the flexural performance of woven E-glass/polyester-reinforced composites. *J Compos Mater* 2015. DOI: 10.1177/0021998315620478.
- [33] Fancey KS, Fazal A. Prestressed polymeric matrix composites: Longevity aspects. *Polym Compos*, 2015; 37(3):2092-7.
- [34] Pang JWC, Fancey KS. The flexural stiffness characteristics of viscoelastically prestressed polymeric matrix composites. *Compos Part A* 2009; 40(6-7):784-90.
- [35] Fazal A, Fancey KS. Viscoelastically generated prestress from ultra-high molecular weight polyethylene fibres. *J Mater Sci* 2013; 48(16):5559-70.
- [36] Fazal A, Fancey KS. UHMWPE fibre-based composites: Prestress-induced enhancement of impact properties. *Compos Part B* 2014; 66:1-6.
- [37] Wang B, Fancey KS. Towards optimisation of load-time conditions for producing viscoelastically prestressed polymeric matrix composites. *Compos Part B* 2016; 87:336-42.
- [38] Fazal A, Fancey KS. Viscoelastically prestressed polymeric matrix composites – Effects of test span and fibre volume fraction on Charpy impact characteristics. *Compos Part B* 2013; 44(1):472-79.

- [39] Wang B, Fancey KS. A bistable morphing composite using viscoelastically generated prestress. *Mater Lett* 2015; 158:108-10.
- [40] Wang B, Fancey KS. Shape-changing (bistable) composites based on viscoelastically generated prestress. In: *Proceedings of 10th International Conference on Composite Science and Technology (ICCST/10)*. Lisbon, September, 2015. p. 1-9. DOI: 10.13140/RG.2.1.1735.6249.
- [41] Timoshenko S. *Strength of Materials*. New York: Robert E. Krieger Publishing Company; 1976. p. 258-80.
- [42] Precast/Prestressed Concrete Institute. *PCI Design Handbook: precast and prestressed concrete*, 7th Edition. Chicago: PCI; 2008.
- [43] Chen W, Hao H, Chen S. Numerical analysis of prestressed reinforced concrete beam subjected to blast loading. *Mater Design* 2015; 65:662-74.
- [44] Benedikt B, Kumosa M, Predecki PK, Kumosa L, Castelli MG, Sutter JK. An analysis of residual thermal stresses in a unidirectional graphite/PMR-15 composite based on X-ray diffraction measurements. *Compos Sci Technol* 2001; 61(14):1977-94.
- [45] Parlevliet PP, Bersee HE, Beukers A. Residual stresses in thermoplastic composites-A study of the literature-Part I: Formation of residual stresses. *Compos Part A* 2006; 37(11):1847-57.
- [46] Jie L, Shinya A, Lassila LVJ. Composite resin reinforced with pre-tensioned fibers: a three-dimensional finite element study on stress distribution. *Odontology* 2013; 101(1):29-33.
- [47] Pang JWC, Lamin BM, Fancey KS. Force measurement from viscoelastically recovering Nylon 6,6 fibres. *Mater Lett* 2008; 62(10-11):1693-96.
- [48] Fancey KS. Prestressed polymeric composites produced by viscoelastically strained nylon 6,6 fibre reinforcement. *J Reinf Plast Compos* 2000; 19(15):1251-66.
- [49] Pang JWC, Fancey KS. An investigation into the long-term viscoelastic recovery of Nylon 6,6 fibres through accelerated ageing. *Mater Sci Eng A* 2006; 431(1-2):100-5.
- [50] Goodfellow Cambridge Ltd. Polyamide - Nylon 6,6 data sheet. [Accessed July 2015]; Available from: <http://www.goodfellow.com>.
- [51] Aly MF, Goda IGM, Hassan GA. Experimental investigation of the dynamic characteristics of laminated composite beams. *Int J Mech & Mech Eng* 2010; 10(3):41-8.
- [52] AZO Materials. E-glass fibre properties. [Accessed November 2015]; Available from: <http://www.azom.com/properties.aspx?ArticleID=764>.
- [53] Voigt W. Ueber die Beziehung zwischen den beiden Elasticitätsconstanten isotroper Körper. *Annalen der Physik* 1889; 274(12):573-87.
- [54] Reuss A. Berechnung der Fließgrenze von Mischkristallen auf Grund der Plastizitätsbedingung für Einkristalle. *ZAMM-Z Angew Math Me* 1929; 9(1):49-58.
- [55] Jones RM. *Mechanics of Composite Materials*. New York: McGraw-Hill Book Co.; 1975.
- [56] Krenchel H. *Fibre reinforcement*. Copenhagen: Akademisk Forlag; 1964.
- [57] Davallo M, Pasdar H. Comparison of mechanical properties of glass-polyester composites formed by resin transfer molding and hand lay-up technique. *Int J ChemTech Res* 2009; 1(3):470-5.

- [58] Rodríguez E, Petrucci R, Puglia D, Kenny JM, Vázquez A. Characterization of composites based on natural and glass fibers obtained by vacuum infusion. *J Compos Mater* 2005; 39(3):265-82.
- [59] Dai F, Li H, Du S. A multi-stable lattice structure and its snap-through behavior among multiple states. *Compos Struct* 2013; 97:56-63.
- [60] Wang B. Viscoelastically prestressed composites: towards process optimisation and application to morphing structures. PhD Thesis. University of Hull: United Kingdom; 2016.
- [61] Lee JG, Ryu J, Kim SW, Koh JS, Cho KJ, Cho M. Effect of initial tool-plate curvature on snap-through load of unsymmetric laminated cross-ply bistable composites. *Compos Struct* 2015; 122:82-91.

## Figure captions

- Fig. 1. Schematic representation of bistable VPPMC principles, showing the VPPMC assembled structure in both states (Shapes I and II) and also the prestress-generated deflection  $\delta$  in accordance with Eq. (2). Redrawn from [39].
- Fig. 2. Schematic three point bending set-up used to evaluate the snap-through characteristics of the VPPMC-based test samples; a point-force loading indenter was adopted.
- Fig. 3. Effective modulus of glass fibre mat reinforced polyester resin composite as a function of fibre volume fraction. The dashed line represents Eq. (5) with  $k = 3/8$ , showing good agreement with published data [57, 58]; the black solid lines represent the standard ‘rule of mixtures’ relationships, i.e. Eqs. (3) and (4).
- Fig. 4. Boundary and loading conditions on the plate: (a) constraints applied in Step-1; (b) constraints applied in Step-2.
- Fig. 5. An assembled VPPMC-based bistable sample (test), compared with the equivalent control (no prestress) sample.
- Fig. 6. Snap-through load response of the bistable composite assemblies in both directions with a test speed of 60 mm/min.
- Fig. 7. Localised ripple effect during the snap-through tests, showing the critical moment (a) before and (b) after the snap-through event.
- Fig. 8. Loading history for the FE analysis: (a) temperature change during the FE process; (b) displacement change of the indenter through the modelling period.
- Fig. 9. Simulated stable shape in the  $y$ -direction generated after Step-1: (a) stress distribution within the whole bistable structure; (b) stress distribution within the fibreglass mid-layer.
- Fig. 10. Snap-through process of the bistable structure through the FE model: (a) original plate; (b) first stable cylindrical shape in the  $y$ -direction; (c) second stable cylindrical shape in the  $x$ -direction.
- Fig. 11. Reaction force versus indenter displacement within the snap-through process for FE simulation, compared to the experimental data from Section 5.2.
- Fig. 12. Development of the snap-through process for a bistable structure panel with pre-defined deflection values,  $\delta$ . Dashed lines show the change in maximum load and critical displacement for snap-through behaviour; inserted figures show the corresponding deformation (contours) that occur (a) before and (b) after the critical moment of each feature.
- Fig. 13. FE results showing load-displacement curves for bistable structures with different modulus ratios,  $R_E$ .
- Fig. 14. FE results of the modulus ratio effect on peak load, critical displacement and model deflection; dashed lines show the trends.

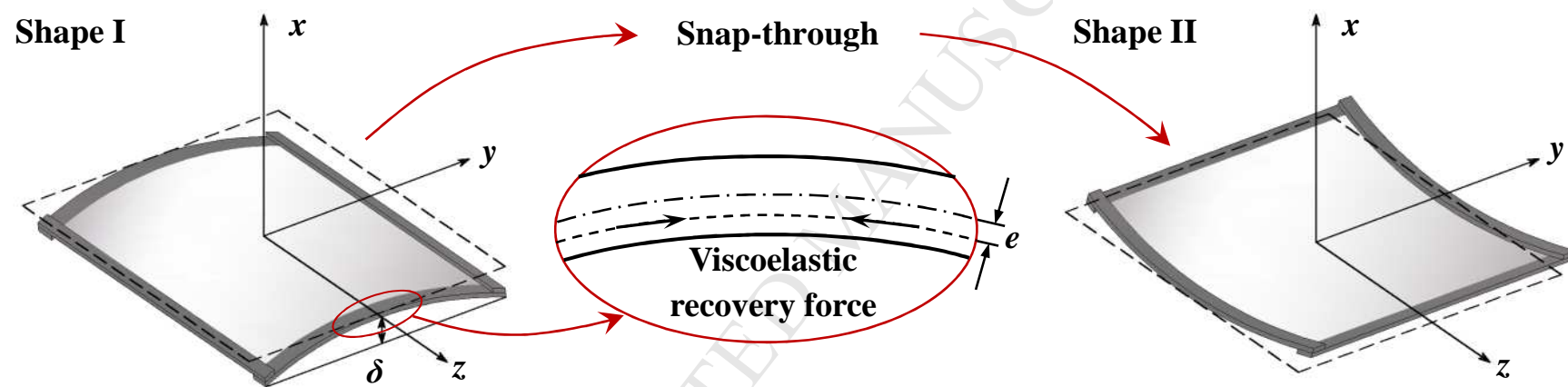


Fig. 1.

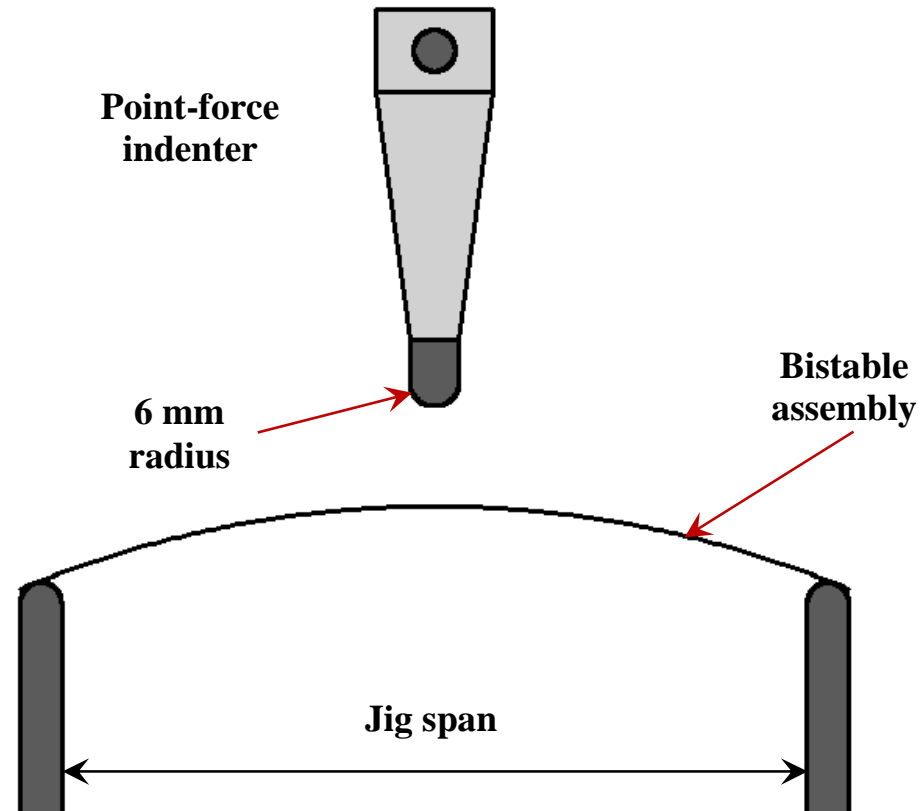


Fig. 2.

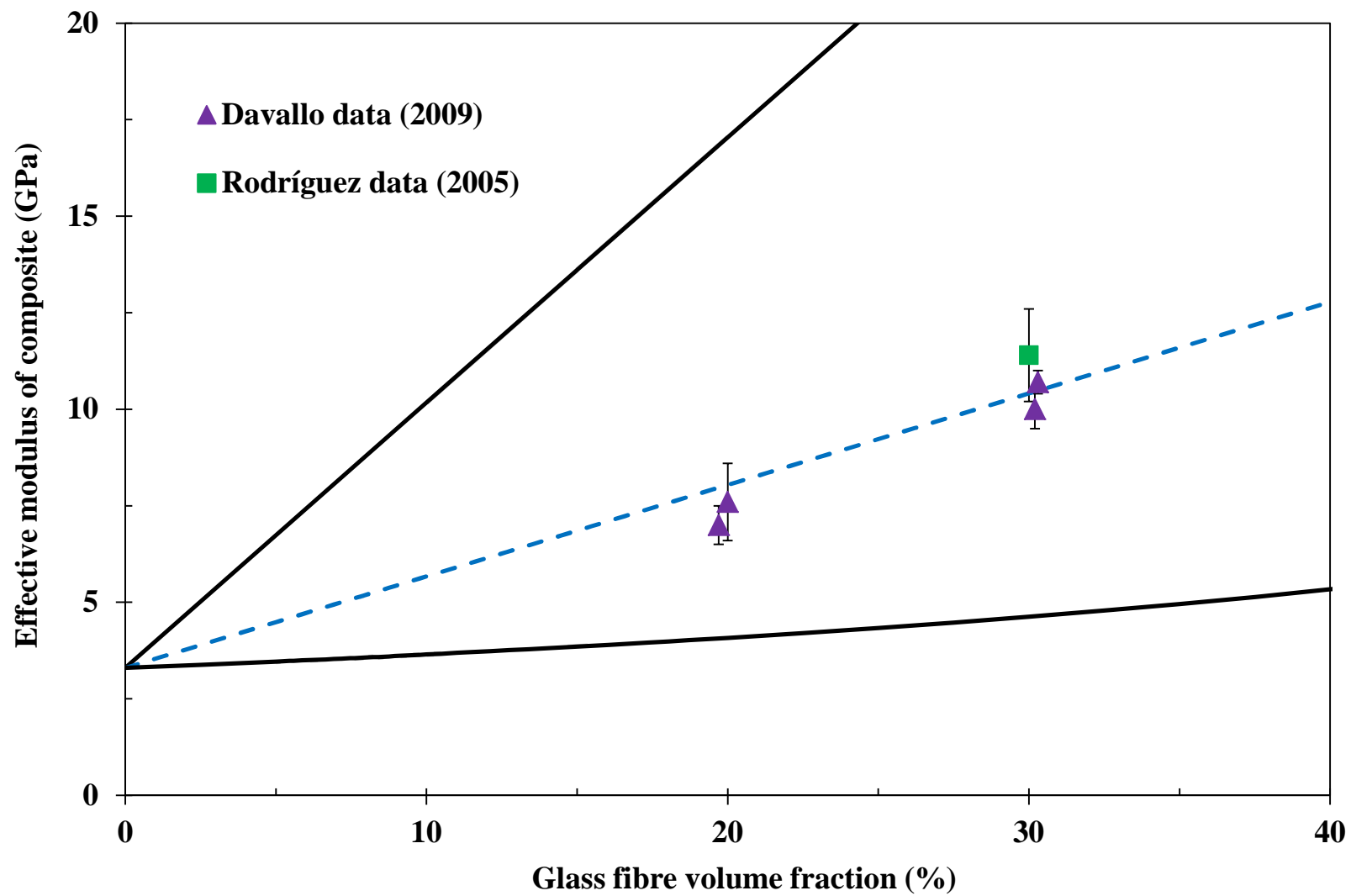


Fig. 3.

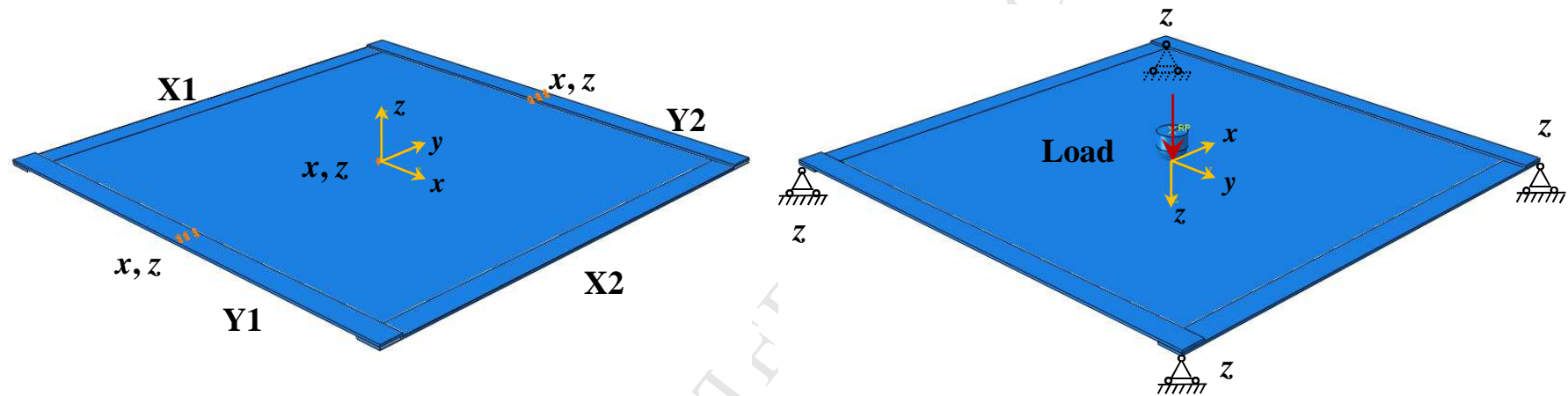


Fig. 4.

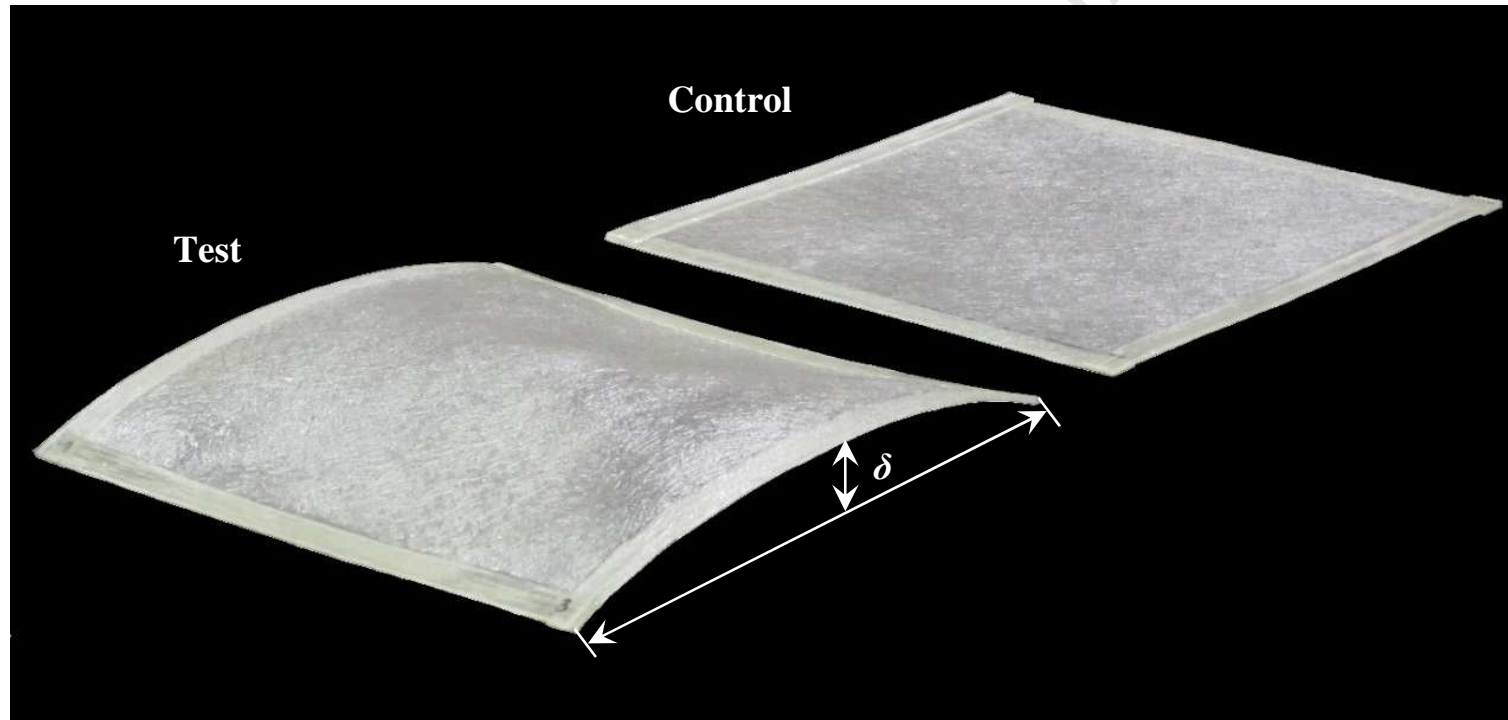


Fig.5.

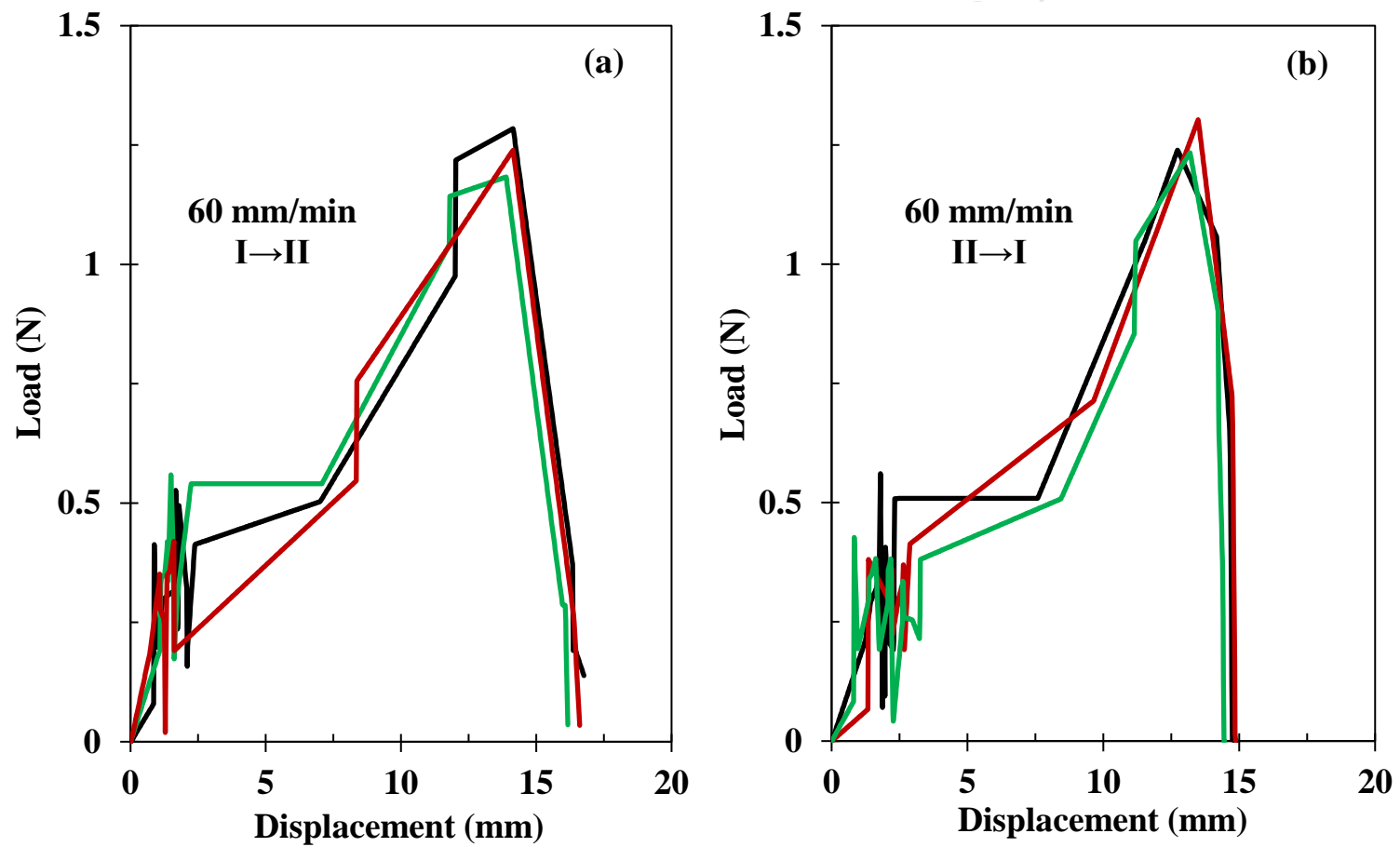


Fig. 6.

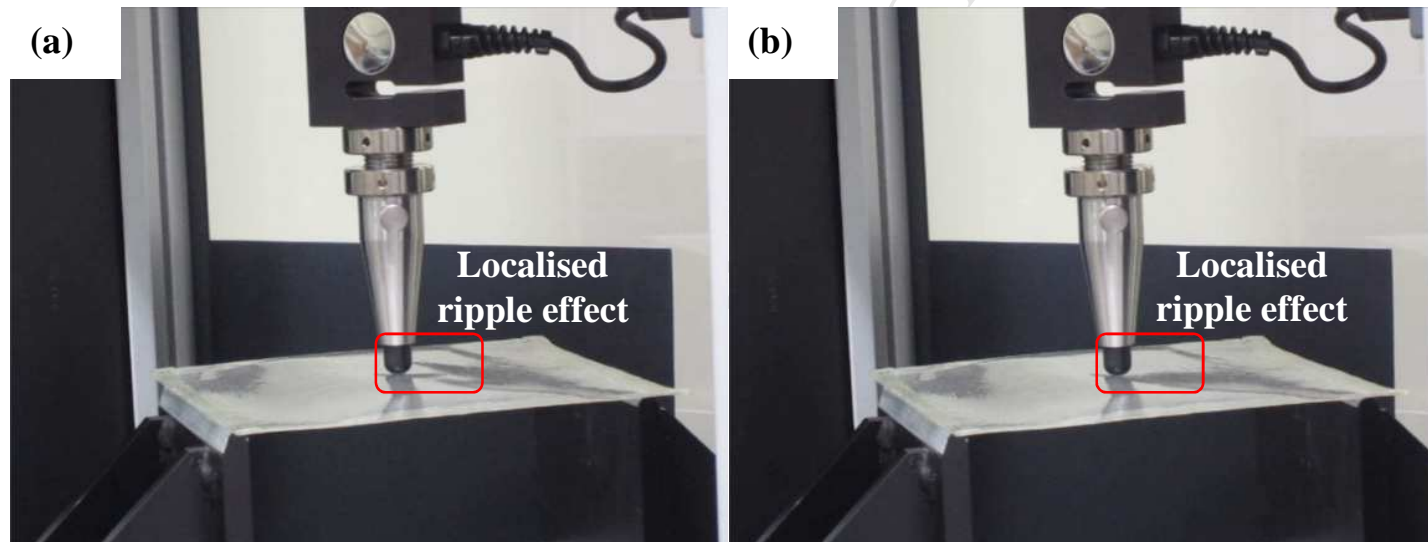


Fig. 7.

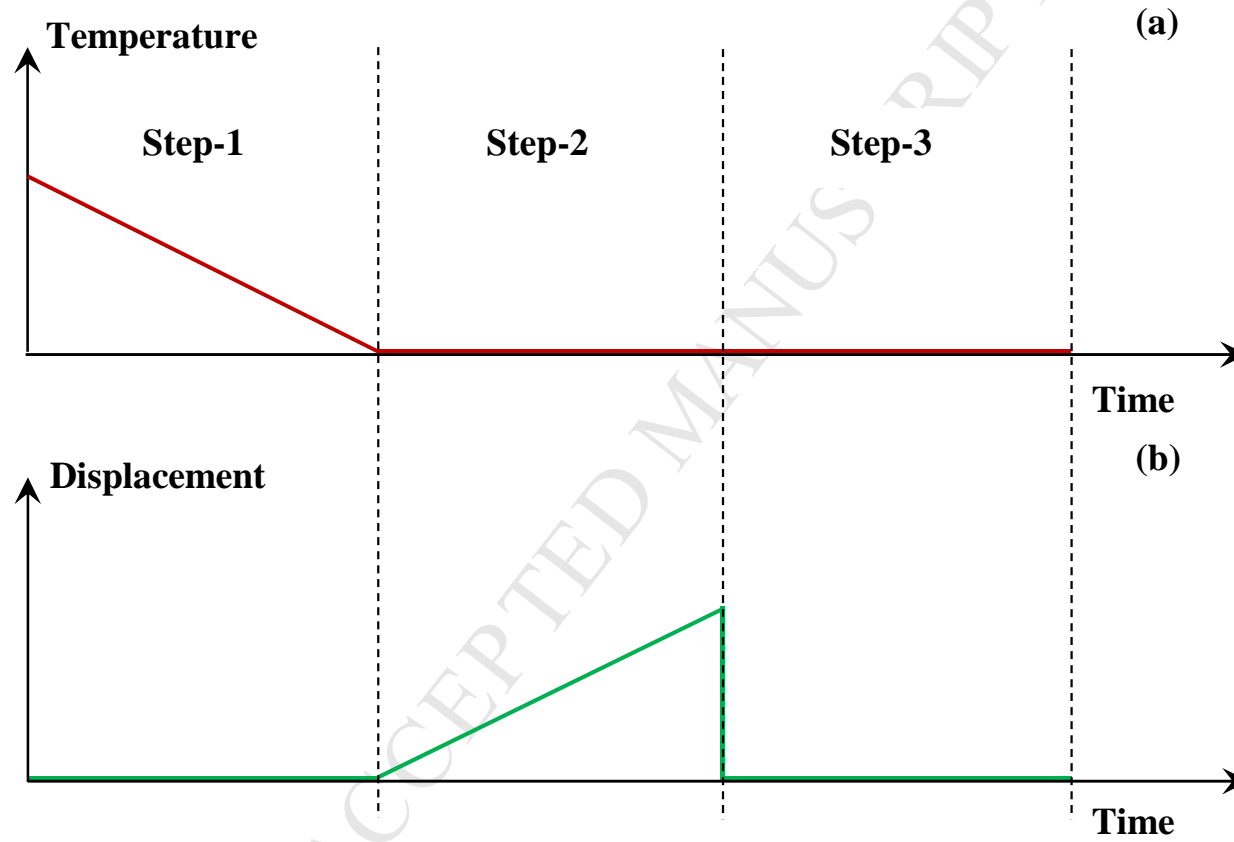


Fig. 8.

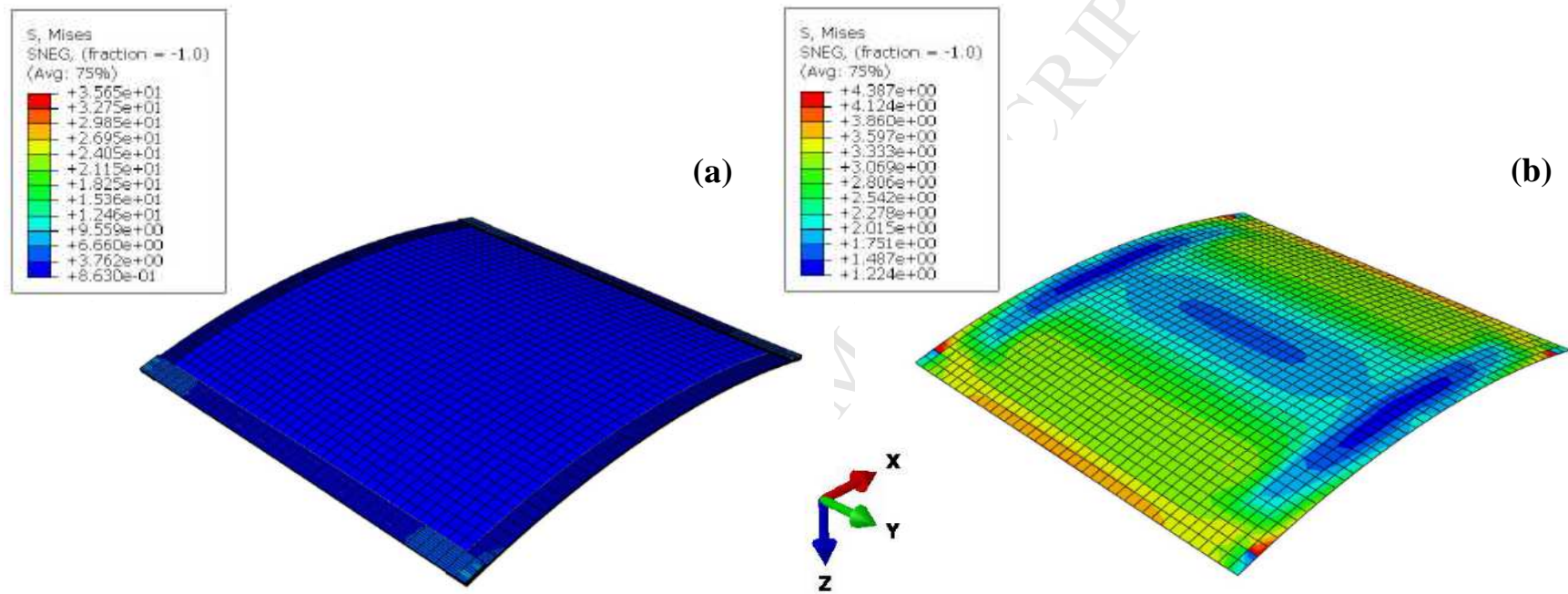


Fig. 9.

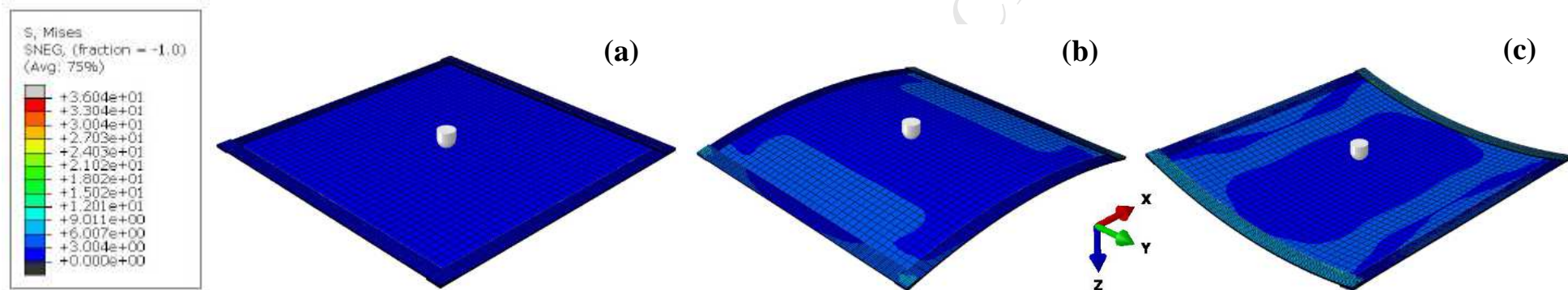


Fig. 10.

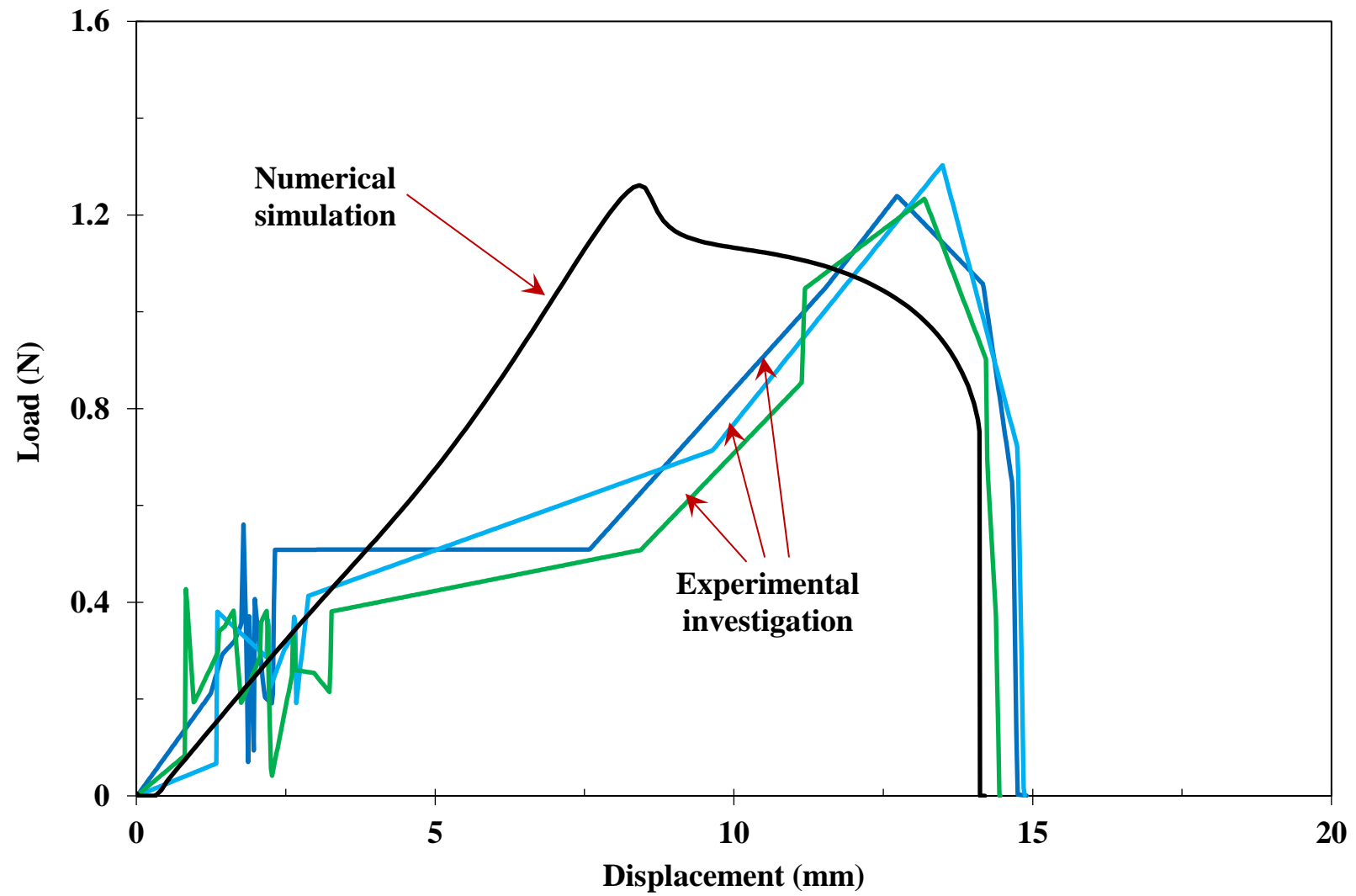


Fig. 11.

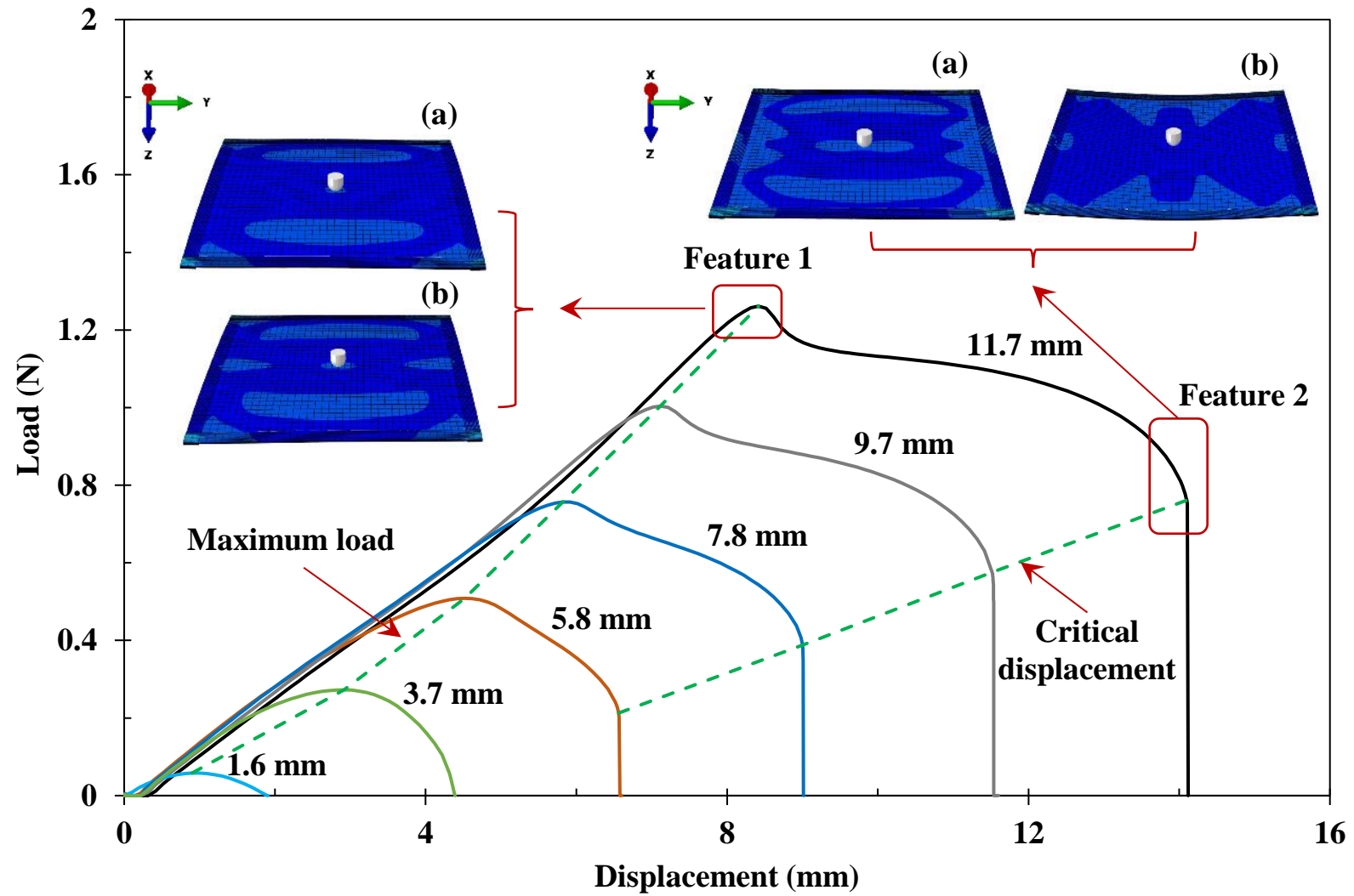


Fig. 12.

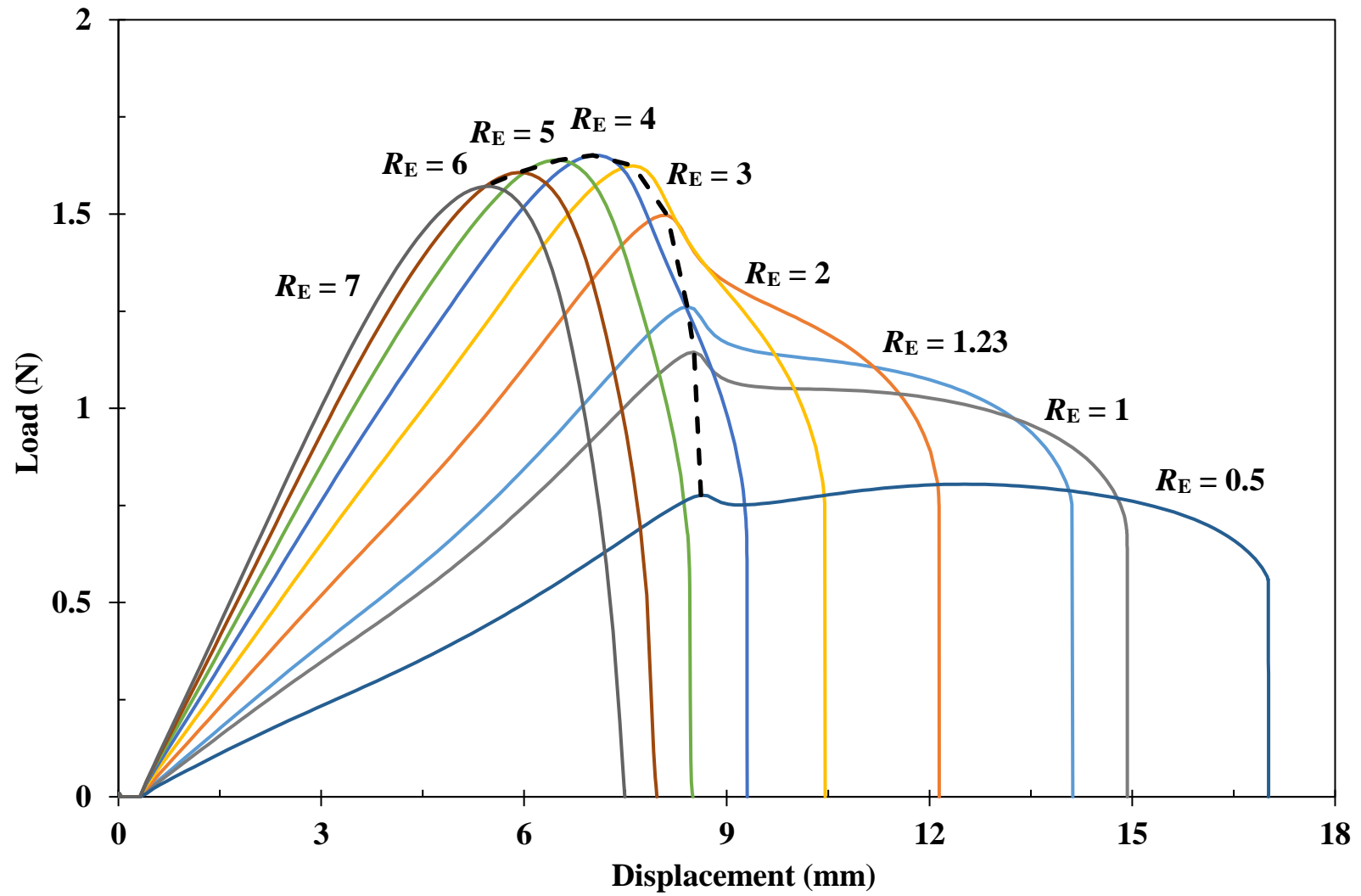


Fig. 13.

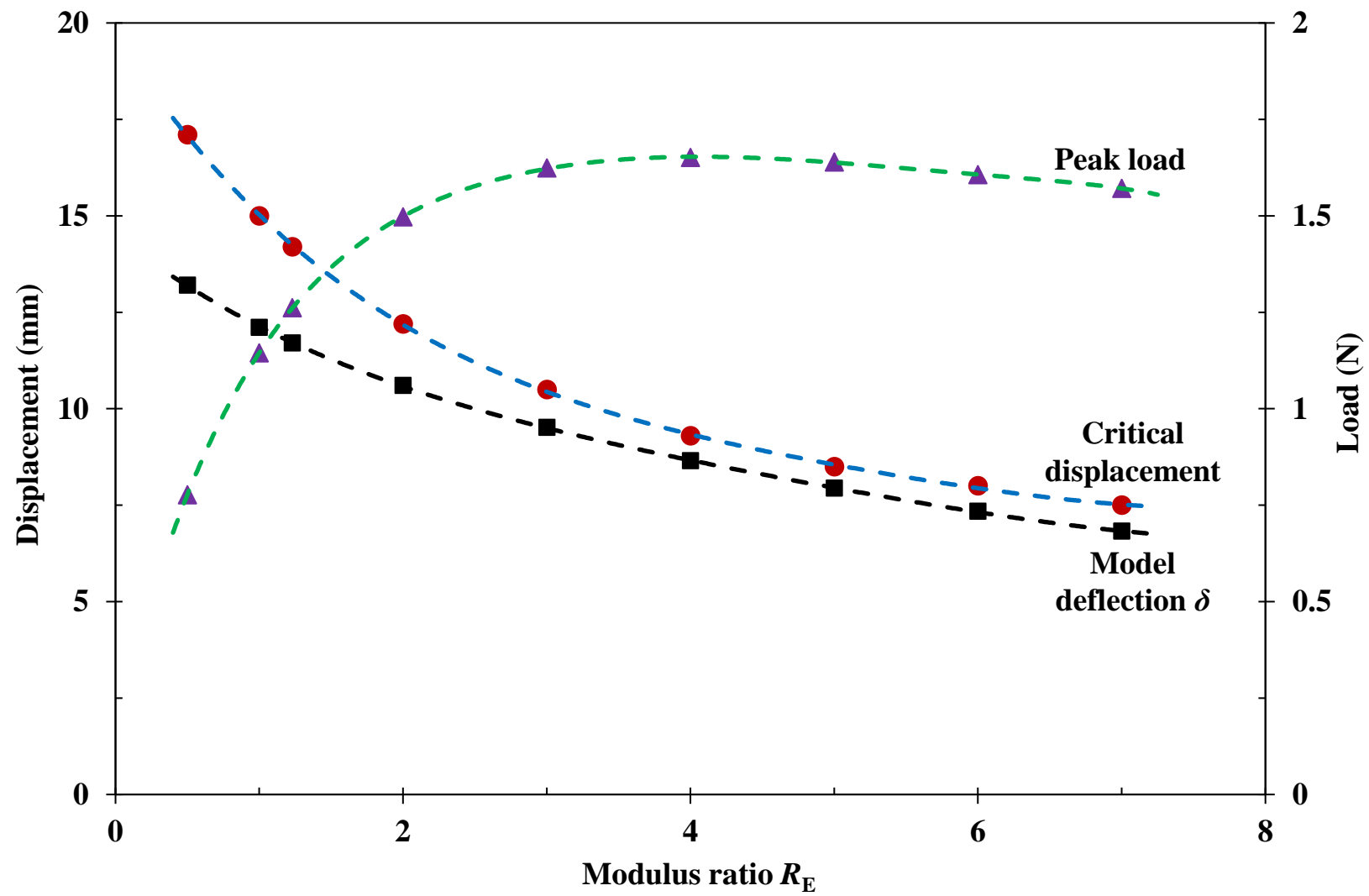


Fig. 14.